

A study of the cross-correlation and time lag in black hole X-ray binary XTE J1859+226

Songpeng Pei^{1,2} • Guoqiang Ding¹ • Zhibing Li¹ •
Yajuan Lei³ • Rai Yuen^{1,4} • Jinlu Qu⁵

© Springer-Verlag ●●●

Abstract

With Rossi X-ray Timing Explorer (RXTE) data, we systematically study the cross-correlation and time lag in all spectral states of black hole X-ray binary (BHXB) XTE J1859+226 in detail during its entire 1999–2000 outburst that lasted for 166 days. Anti-correlations and positive correlations and their respective soft and hard X-ray lags are only detected in the first 100 days of the outburst when the luminosity is high. This suggests that the cross-correlations may be related to high luminosity. Positive correlations are detected in every state of XTE J1859+226, viz., hard state, hard-intermediate state (HIMS), soft-intermediate state (SIMS) and soft state. However, anti-correlations are only detected in HIMS and SIMS, anti-correlated hard lags are only detected in SIMS, while anti-correlated soft lags are detected in both HIMS and SIMS. Moreover, the ratio of the observations with anti-correlated soft lags to hard lags detected in XTE J1859+226 is significantly different from that in neutron star low-mass X-ray binaries (NS LMXBs). So far, anti-correlations are never de-

tected in the soft state of BHXBs but detected in every branch or state of NS LMXBs. This may be due to the origin of soft seed photons in BHXBs is confined to the accretion disk and, for NS LMXBs, from both accretion disk and the surface of the NS. We notice that the timescale of anti-correlated time lags detected in XTE J1859+226 is similar with that of other BHXBs and NS LMXBs. We suggest that anti-correlated soft lag detected in BHXB may result from fluctuation in the accretion disk as well as NS LMXB.

Keywords accretion, accretion discs – X-rays: binaries – black hole physics – stars: individual (XTE J1859+226)

1 Introduction

X-ray binaries (XRBs) are mass-exchange binary systems consist of a compact object (an accreting object primary) and a companion star (a nondegenerate secondary star). The X-rays are produced by the compact object (the accretor) accretes falling matter from the companion star (the donor). Based on the mass of the donor star, XRBs are further subdivided into low-mass X-ray binaries (LMXBs) ($M_{donor} \leq 1 M_{\odot}$) and high-mass X-ray binaries (HMXBs) ($M_{donor} \geq 10 M_{\odot}$) (Lewin & van der Klis 2006; Colpi et al. 2009). Depending on whether the compact object is a black hole (BH) or a neutron star (NS), XRBs can be further subdivided into black hole X-ray binaries (BHXBs) and NS XRBs. Based on the spectral properties and color-color diagrams (CCDs), NS LMXBs can be classified into two subtypes, viz., atoll sources and Z-sources (Hasinger & van der Klis 1989).

It is well known that the X-ray energy spectra of BHXBs often consist of a thermal (soft) and a non-thermal (hard) component. The thermal component,

Songpeng Pei
Guoqiang Ding
Zhibing Li
Yajuan Lei
Rai Yuen
Jinlu Qu

¹Xinjiang Astronomical Observatory, Chinese Academy of Sciences, 150, Science 1-Street, Urumqi, Xinjiang 830011, China

²University of Chinese Academy of Sciences, 19A Yuquan Road, Beijing 100049, China

³National Astronomical Observatories, Chinese Academy of Sciences, Beijing 100012, China

⁴Key Laboratory of Radio Astronomy, Chinese Academy of Sciences, Urumqi, Xinjiang, 830011, China

⁵Key Laboratory for Particle Astrophysics, Institute of High Energy Physics, Chinese Academy of Sciences, Beijing 100049, China

which originates from the inner accretion disk, is well modeled by a multitemperature blackbody. The non-thermal component is usually modeled as a power law (PL), and it is generally believed that it results from the Comptonization of soft photons (thermal component) in a hot corona (Compton cloud) and from the jet (Markoff & Nowak 2004; Markoff, Nowak, & Wilms 2005).

Based on the evolution of spectral and timing properties, the spectral states of BHXBs can be divided into five states: quiescent state, low/hard state (LHS), intermediate state (IMS), high/soft state (HSS), and very high state (VHS) (Remillard 2005; Remillard & McClintock 2006; Belloni 2010). McClintock & Remillard (2006), however, used a quantitative three-state description to define the spectral states of BHXBs. The three states are hard, thermal, and steep power law (SPL) states, which are comparable with LHS, HSS and VHS, respectively (Done, Gierliński, & Kubota 2007; Belloni 2010; Remillard & McClintock 2006). VHS and IMS are at different luminosities, while they are usually taken as one and the same transition state between the LHS and HSS. This is because they have similar spectral and timing behaviors, and their amalgamative state can be divided into hard-intermediate state (HIMS) and soft-intermediate state (SIMS) (Done, Gierliński, & Kubota 2007; Belloni 2010). Most states are over wide and overlapping in luminosity, which means that ‘low’, ‘high’ and ‘very high’ have lost most of their significance, so the spectral states of BHXBs in the outburst can be divided into four basic states: hard state, HIMS, SIMS, and soft state (Homan & Belloni 2005; Debnath et al. 2008; Motta, Belloni, & Homan 2009; Dunn et al. 2010; Nandi et al. 2012).

Spectral and timing analyses are the most important means to study XRBs. In particular, the timing analysis has been widely used for investigation of the underlying geometrical structure and dynamics of the accretion disk and the radiation mechanism of XRBs. Cross-correlation analysis is an important tool to carry out timing study from which cross-correlation functions (CCFs) and time lags between different energy bands are obtained. Positive correlations (anti-correlations) between low and high energy band light curves correspond to positive (negative) cross-correlation coefficients (CCCs). The correlation between two different energy band light curves is defined as ambiguous correlation when their CCFs do not present obvious correlation. Soft time lag implies that the higher energy photons lead the lower energy photons, whereas hard time lag means that the higher energy photons reach behind.

If hard time lag is detected in one observation owning the anti-correlation, that hard time lag is called anti-correlated hard lag, and the reverse is anti-correlated soft lag. Similarly, the time lags can be divided into positive correlation hard lags and positive correlation soft lags for observations with positive correlation.

Choudhury & Rao (2004) first performed cross-correlation analysis on BHXB Cyg X-3 to study the correlations and time lags between the low and high X-ray energy bands. They first detected anti-correlated long time-scale hard X-ray lags in the hard state of Cyg X-3, which range from hundreds of seconds to about one thousand seconds. Since then cross-correlation analysis has been widely used for study of the timing properties of XRBs. Tens of seconds to over 1500 seconds anti-correlated time lags were detected in the IMS of other BHXBs that are GRS 1915+105 (Choudhury et al. 2005), XTE J1550-564, 4U 1630-47 (Sriram et al. 2007), H1743-322 (Sriram, Agrawal, & Raghurama Rao 2009) and GX 339-4 (Sriram, Rao, & Choi 2010). Similar kinds of anti-correlated time lags were observed in six other NS LMXBs, including four Z-sources (Cyg X-2 (Lei et al. 2008), GX 5-1 (Sriram, Choi, & Rao 2012), XTE J1701-462 (Wang et al. 2014) and GX 349+2 (Ding et al. 2016)) and two atoll sources (4U 1735-44 (Lei et al. 2013) and 4U 1608-52 (Lei et al. 2014)), and positive correlated time lags were also observed in them. Furthermore, the evolution of the cross-correlation along the branches in the CCD or hardness intensity diagram (HID) was studied for the six NS LMXBs. Based on the systematic cross-correlation analysis of 4U 1608-52 (atoll source), Lei et al. (2014) proposed that the distribution of the cross-correlations on the CCDs might be in evolution with the luminosity of the source. Similar results were also found in a Z-source XTE J1701-462 by Wang et al. (2014). However, the evolution of cross-correlations along with the luminosity of the source and the spectral states has never been investigated in BHXBs, nor has the cross-correlation analysis been performed on a whole outburst of BHXBs.

XTE J1859+226 is a BHXB which was first detected by the All-Sky Monitor (ASM) of Rossi X-Ray Timing Explorer (RXTE) during its outburst on Oct 9, 1999 (MJD 51460) (Wood et al. 1999). Shaposhnikov & Titarchuk (2009) used correlation scaling method to upgrade the source distance from 6–11 kpc (Hynes et al. 2002; Zurita et al. 2002) to 4.2 ± 0.5 kpc with the state transition data of RXTE observations. Based on the optical photometry and spectroscopy observations of transient source XTE J1859+226, Corral-Santana et al. (2011) obtained an

orbital period of 6.58 ± 0.05 hr, radial velocity amplitude of $K_2 = 541 \pm 70$ km s^{-1} for the companion star, mass function $f(M) = 4.5 \pm 0.6 M_\odot$, and a lower mass limit of $5.42 M_\odot$. Markwardt, Marshall, & Swank (1999) detected low-frequency quasi-periodic oscillations (LFQPOs) and Cui et al. (2000) discovered high-frequency quasi-periodic oscillations (HFQPOs) in the X-ray intensity of XTE J1859+226. Using the RXTE/BeppoSAX data, Farinelli et al. (2013) discovered strong positive correlation between the root mean square (RMS) and the fraction of Comptonized seed photons. Using RXTE data obtained during the whole 1999–2000 outburst, Radhika & Nandi (2014) studied the evolution of spectral and temporal properties associated with different spectral states to explore the accretion dynamics. Results from study for the variation of spectral and temporal properties show that the whole outburst of XTE J1859+226 evolved through seven state transitions: hard state \rightarrow HIMS \rightarrow SIMS \rightarrow soft state \rightarrow SIMS \rightarrow HIMS \rightarrow hard state (Radhika & Nandi 2014).

The motivation for this work is to study in detail the evolution of cross-correlations and long-term time lags along with the spectral states of BHXBs. The evolution of correlations and long-term time lags along with the spectral states of BHXBs has never been investigated, and we select BHXB XTE J1859+226 as it evolved through a sequence of spectral states during the 1999–2000 outburst (Radhika & Nandi 2014). The observations and data reduction are described in Section 2. The results are shown in Section 3, and discussion is present in Section 4. Finally, our conclusions are drawn in Section 5.

2 OBSERVATIONS AND DATA REDUCTION

In HEASARC database, there are 129 available observations generated by the two onboard detectors of RXTE, viz., Proportional Counter Array (PCA) and High Energy X-ray Timing Experiment (HEXTE). We excluded observations with exposure time less than 1000 s and two observations that are out of the outburst. The remaining 114 observations span over 164 days from October 11, 1999 (MJD 51462.76) to March 23, 2000 (MJD 51626.59). Based on the 114 observations, we study the characteristics of XTE J1859+226 covering the entire duration of the single outburst. Given that the light curves from some observations are discontinued, we follow Sriram, Choi, & Rao (2012); Lei et al. (2013, 2014); Wang et al. (2014) by dividing these observations into several individual segments with

uninterrupted duration (> 1000 s). We finally obtain 140 observations/segments.

HEASOFT v 6.17, XSPEC v 12.9, and XRONOS v 5.22 are used for data reduction. Only the PCA Standard 2 form of data are used with 32 s bin size. The GTI files are created based on the criteria that the earth elevation angle is $> 10^\circ$ and the spacecraft pointing offset is $< 0.02^\circ$. For the observation/segment whose X-ray intensity is greater than $40 \text{ counts s}^{-1} \text{ PCU}^{-1}$, the bright background model (`pca_bkgd_cmbrightvle_eMv20051128.mdl`) is used, and for the others, the faint background model (`pca_bkgd_cmfaintl7_eMv20051128.mdl`) is used. We then use PCABACKEST v 4.0 to create PCA background files for extracting the background light curves.

PCU0 and PCU2 are used for the cross-correlation and spectra analyses as they are the only PCUs that always work for the 114 observations. CCF is then generated with the XRONOS program “*cross-cor*” using the soft (2–5 keV) and hard (20–50 keV) (Sriram et al. 2007) energy bands background-subtracted light curves. Following Sriram et al. (2007) and Sriram, Choi, & Rao (2012), we fit the peak of CCFs with an Gaussian function to obtain the CCCs and time lags at 90 percent confidence level where the errors are obtained based on the criterion of $\Delta\chi^2 = 2.7$. Following Lei et al. (2008, 2013, 2014), the background-subtracted spectra from the soft regions (the hardness ratio is 10% less than the average at 20–50 keV/2–5 keV) and from the hard regions (the hardness ratio is 10% more than the average at 20–50 keV/2–5 keV) are used to study spectral change.

To check whether the values of time lags and CCCs change if the time bin changes, we also perform cross-correlation analysis on the PCA Standard 2 form of data with time bin of 64 s besides 32 s bin size. It turns out that the time lags do not change while the values of CCCs get a little larger when the time bin size is changed from 32 s to 64 s. Fig. 1 shows a representative example of the CCFs with the 32 s and 64 s bin size of an observation. To be consistent with other works, the time lags and CCCs are obtained from 32 s bin size of PCA Standard 2 form of data in this work.

Light curve and HID are used for study of the evolution of cross-correlations and time lags. The intensity is defined as the background subtracted light curve of 2–20 keV, the hardness is defined as the count-rate ratio of 6–20 keV/2–6 keV, and only data of PCU2 are used, which are the same as given by Radhika & Nandi (2014).

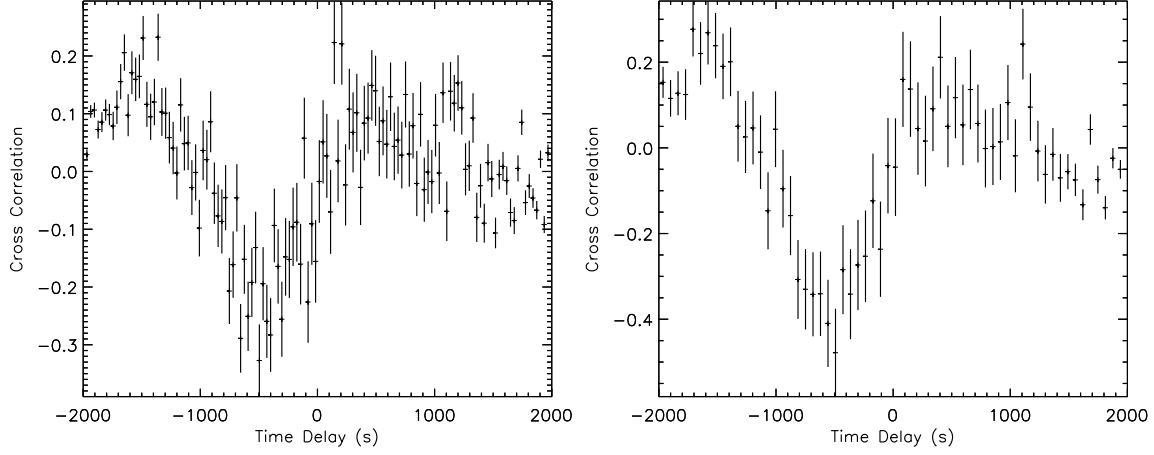


Fig. 1 Left: the CCFs of observation ID (ObsID) 40124-01-61-01 with time bin of 32 s, and the derived values of CCC and time lag are -0.28 ± 0.05 and -501 ± 63 s, respectively. Right: the CCFs of ObsID 40124-01-61-01 with time bin of 64 s, and the derived values of CCC and time lag are -0.37 ± 0.03 and -498 ± 57 s, respectively.

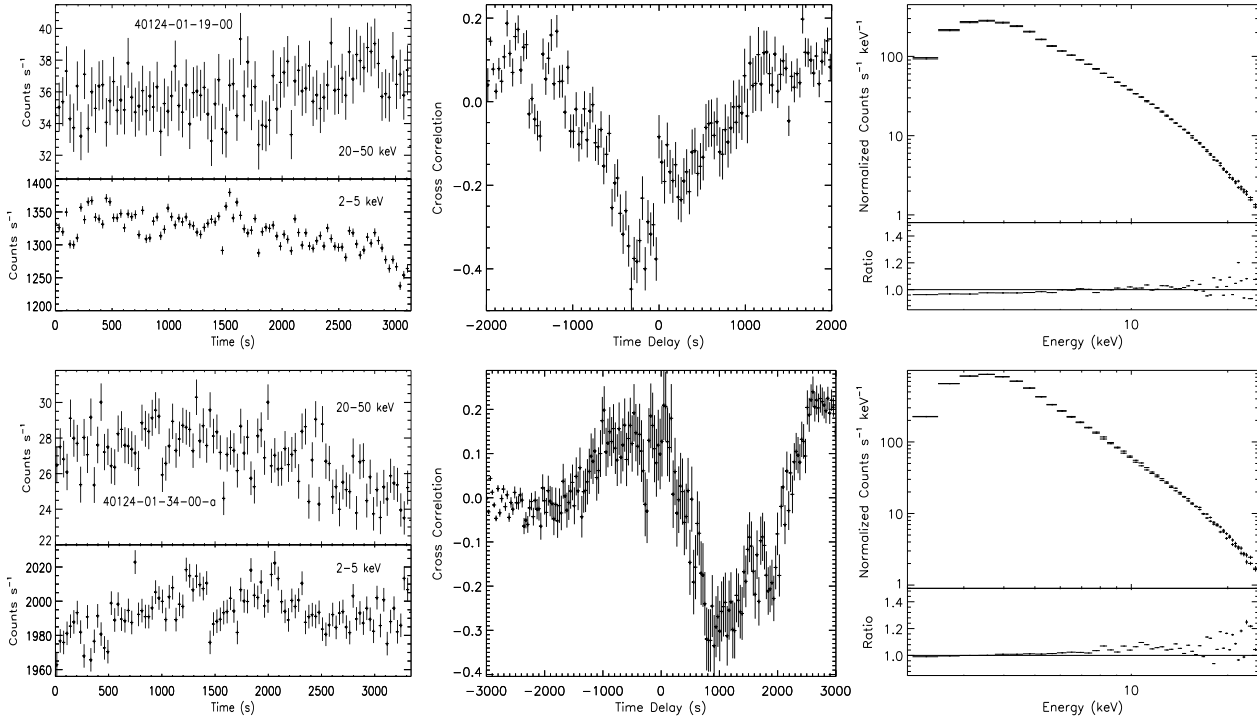


Fig. 2 Left: the PCA hard light curves (20-50 keV) and soft light curves (2-5 keV) for which anti-correlated soft lag (upper panel) and hard lag (lower panel) are detected. Middle: the corresponding cross-correlation functions. Right: the hard region spectra and soft region spectra and their ratio, which show spectral pivoting.

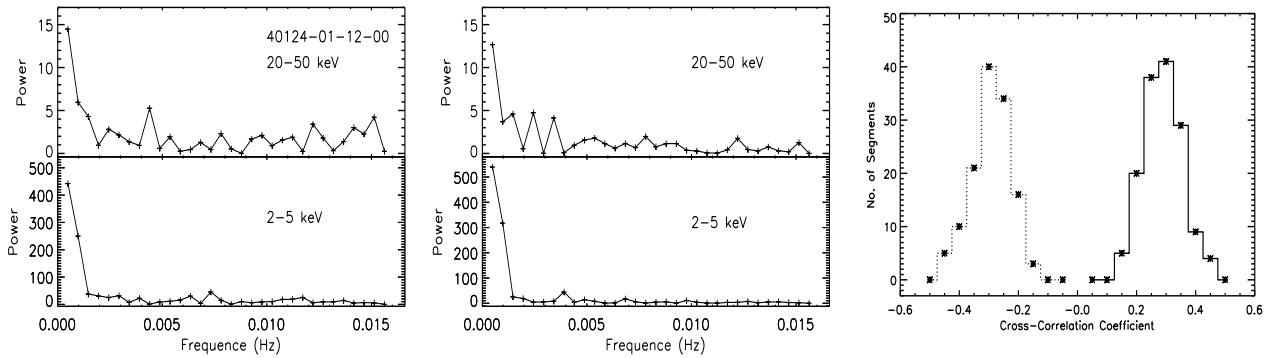


Fig. 3 Left: the PDS of hard light curve (20-50 keV) and soft light curve (2-5 keV) of 40124-01-12-00. Middle: the PDS of the two simulated light curves (the same duration as 40124-01-12-00). Right: histogram of the CCCs obtained from the simulated light curves. The CCCs of the anti-correlations (dotted line) and positive correlations (solid line) vs. the number of segments.

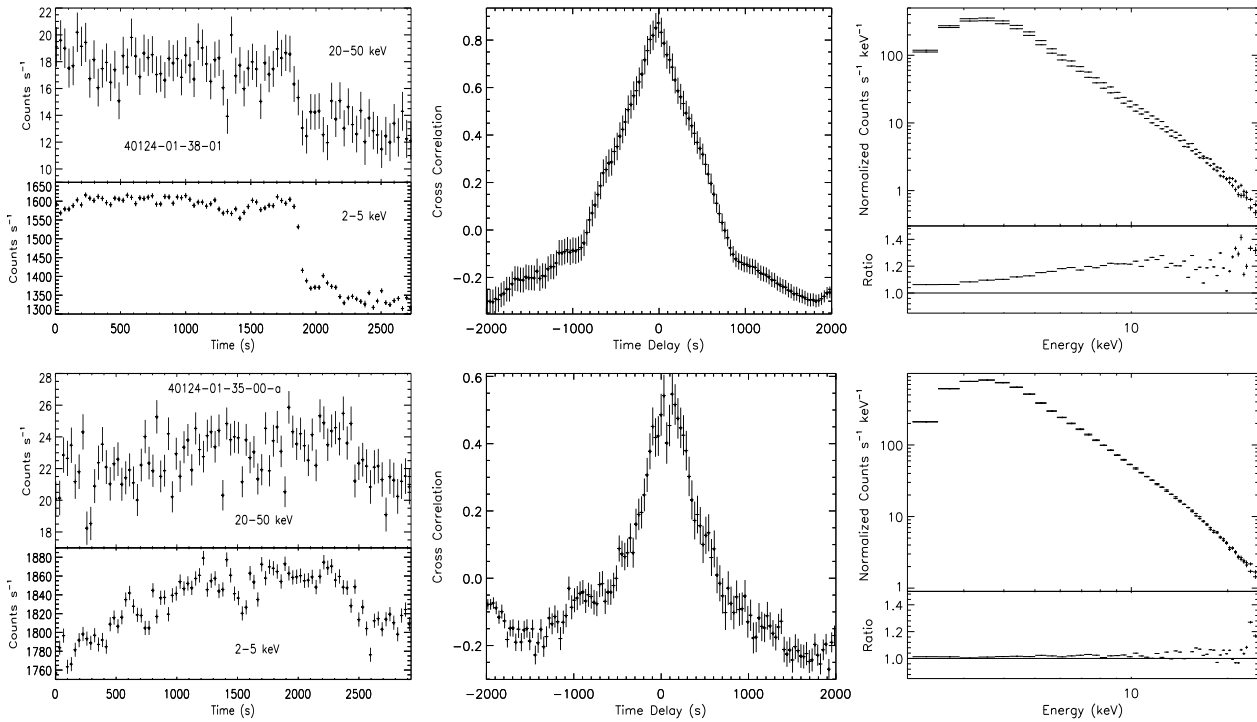


Fig. 4 Left: the PCA hard light curves (20-50 keV) and soft light curves (2-5 keV) for which positive correlated soft lag (upper panel) and hard lag (lower panel) are detected. Middle: the corresponding cross-correlation functions. Right: the hard region spectra and soft region spectra and their ratio, which do not show spectral pivoting.

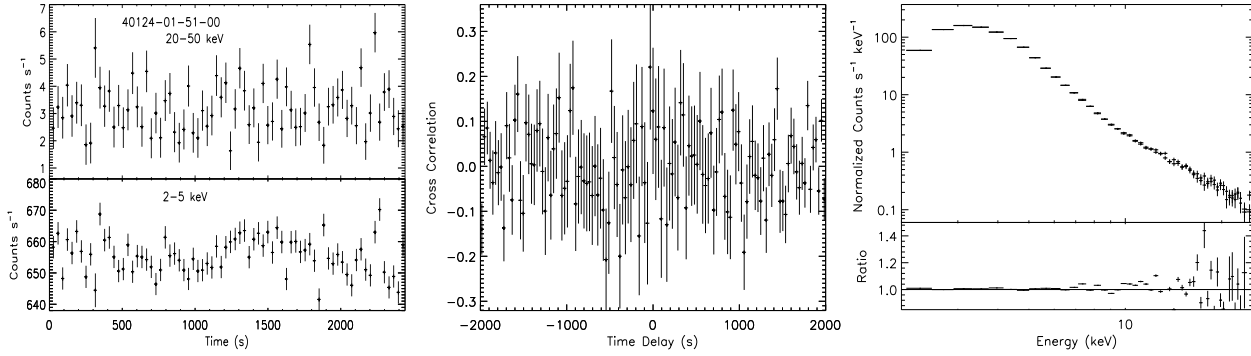


Fig. 5 Left: the PCA hard light curves (20–50 keV) and soft light curves (2–5 keV) showing a typical ambiguous correlation. Middle: the corresponding cross-correlation functions. Right: the hard region spectra and soft region spectra and their ratio, which do not show spectral pivoting.

3 RESULTS

After performing cross-correlation analysis on all the 140 observations/segments during the 1999–2000 outburst of XTE J1859+226, both anti-correlations and positive correlations with soft or hard X-ray long time-scale lags are detected.

9 out of 140 observations/segments display anti-correlations in HIMS and SIMS as shown in Table 1. Among the observations with anti-correlations, soft lags and hard lags are detected in 7 and 2 observations/segments, respectively, where soft lags are located in HIMS and SIMS, and hard lags are located in SIMS (see Table 1). Clearly, the number of the observations/segments with anti-correlation soft lags is more than that with anti-correlation hard lags. Fig. 2 shows a representative example of anti-correlated soft lag (upper panel) and hard lag (lower panel), in which the observations with anti-correlation show spectral pivoting. Spectral pivoting means that the spectral of soft regions and the spectral of hard regions intersect at a pivoting point which corresponds to the point of unit spectral ratio (Rau & Greiner 2003; Choudhury et al. 2003).

To confirm the detected anti-correlation, we follow Sriram, Rao, & Choi (2010); Sriram, Choi, & Rao (2012); Lei et al. (2014) by simulating two long independent light curves (2.24×10^6 s) using the method described in Timmer & Koenig (1995). To obtain the two simulated light curves, we use the parameters of the observation ID (ObsID) 40124-01-12-00 where the highest anti-correlation coefficient (~ -0.42) is detected. For this observation, the mean count rate, standard deviation and power density spectrum (PDS) power-law index β of the soft energy band light curve are 3253.7 counts s^{-1} , 43.2 counts s^{-1} and -1.32 , and the mean count rate, standard deviation and PDS power-law index β of the hard energy band light curve are 44.5 counts s^{-1} , 1.8 counts s^{-1} and -0.83 , respectively.

To obtain the power-law index, a power-law model is used to fit the corresponding PDS. We perform cross-correlation analysis on these two simulated light curves with a bin size of 32 s and a segment length of 3200 s. The histogram of the CCCs is shown in Fig. 3, which indicates that the number of segments with $CCC \leq -0.42$ is low (8 out of 700 segments), more segments show lower level of correlation and more than half of the segments show ambiguous correlation.

Positive correlations are detected in 47 observations/segments. As shown in Table 2, we can see that positive correlations are detected in every state, viz., hard state, HIMS, SIMS and soft state, but mainly in the SIMS. This is due to the fact that most of the observations in the whole outburst are in the SIMS. Table 2 shows that, in the observations with positive correlations, soft lags are detected in 21 observations/segments located in SIMS, and 24 observations/segments with hard lags are found in hard state, HIMS, SIMS and soft state. The example of positive correlated soft lag and hard lag are shown in the upper and lower panels in Fig. 4, respectively, and the observations with positive correlation do not show spectral pivoting.

6.4%, 33.6% and 60.0% of the total 140 observations/segments display anti-correlation, positive correlation and ambiguous correlation, respectively (see Table 3). Fig. 5 shows an example for observation with ambiguous correlation, in which the spectral pivoting is not found. It can be seen from Fig. 6 that positive correlations and anti-correlations distribute alternately on the light curve, and the number of the observations with correlations begins to decrease from the 40th day of the whole outburst. The distribution of the observations with positive correlation in the HID does not have obvious relation with hardness ratio, while the observations with anti-correlations are distributed in the region with moderate hardness ratio, as shown

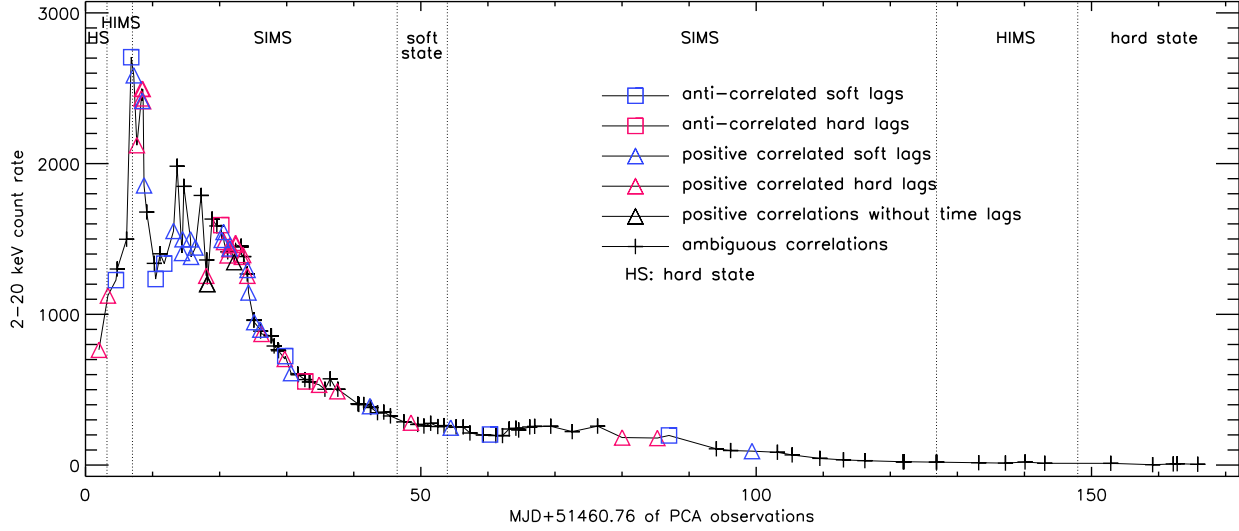


Fig. 6 Plot showing cross-correlation and time lag from the PCA observation for anti-correlated soft lag, anti-correlated hard lag, positive correlated soft lag, positive correlated hard lag, positive correlation without time lag and ambiguous correlation segments, as shown in the legend.

Table 1 Log of all observations (> 1000 s) in which anti-correlations are detected.

ObsID	Start Time	Stop Time	State	CCC	Time Lag (s)
Hard lags					
40124-01-34-00-a	1999-10-30, 00:19	01:17	SIMS ⁽¹⁾	-0.31 ± 0.04	953 ± 65
40124-01-47-00-b	1999-11-11, 12:54	13:34	SIMS	-0.30 ± 0.05	204 ± 87
Soft lags					
40124-01-08-00	1999-10-14, 07:19	08:10	HIMS ⁽²⁾	-0.27 ± 0.06	-143 ± 36
40124-01-12-00	1999-10-16, 13:57	14:30	HIMS	-0.42 ± 0.04	-635 ± 29
40124-01-19-00	1999-10-20, 05:22	06:17	SIMS	-0.39 ± 0.03	-276 ± 32
40124-01-21-00	1999-10-21, 12:04	12:43	SIMS	-0.31 ± 0.04	-120 ± 16
40124-01-44-00-b	1999-11-08, 13:00	13:42	SIMS	-0.25 ± 0.06	-718 ± 75
40124-01-56-00	1999-12-09, 01:58	02:45	SIMS	-0.15 ± 0.03	-124 ± 70
40124-01-61-01	2000-01-04, 18:24	19:17	SIMS	-0.28 ± 0.05	-501 ± 63

Notes. The date, state of the detected anti-correlations on the HID, cross-correlation coefficient and time lag of each observation are listed. We label the segments (> 1000 s) of an observation by ‘a’, ‘b’, and so on.

⁽¹⁾The total rms of the PDS ranges from 7% to 14%, the photon index ranges from 1.9 to 3.2, the disk temperature ranges from 0.70 keV to 0.85 keV, and the fold energy ranges from 108.3 keV to 201.2 keV (Radhika & Nandi 2014).

⁽²⁾The total rms of the PDS ranges from 7% to 24%, the QPO frequency ranges from 3.05 Hz to 5.97 Hz, the photon index ranges from 2.0 to 2.4, the disk temperature ranges from 0.75 keV to 0.85 keV, and the fold energy ranges from 64 keV to 180 keV (Radhika & Nandi 2014).

Table 2 Log of all observations (> 1000 s) in which positive correlations are detected.

ObsID	Start Time	Stop Time	State	CCC	Time Lag (s)
Hard lags					
40124-01-04-00	1999-10-11, 18:25	18:44	hard state ⁽¹⁾	0.43±0.09	170.8±48.2
40124-01-06-00	1999-10-13, 02:37	03:50	HIMS	0.26±0.05	87.3±42.6
40124-01-14-00	1999-10-17, 10:11	11:08	SIMS	0.76±0.04	12.1±3.7
40122-01-01-03	1999-10-18, 02:13	02:57	SIMS	0.39±0.06	13.7±7.5
40122-01-01-02	1999-10-18, 03:49	04:28	SIMS	0.35±0.04	214.7±46.5
40122-01-01-00-a	1999-10-18, 07:01	07:59	SIMS	0.65±0.03	23.3±15.2
40122-01-01-00-b	1999-10-18, 08:36	09:34	SIMS	0.43±0.05	25.7±16.5
40124-01-31-00	1999-10-27, 18:39	19:27	SIMS	0.42±0.04	37.3±19.5
40124-01-34-02	1999-10-30, 10:08	10:48	SIMS	0.46±0.03	38.6±24.8
40124-01-35-01-a	1999-10-30, 22:41	23:07	SIMS	0.28±0.04	107.3±19.2
40124-01-35-00-a	1999-10-31, 05:11	06:02	SIMS	0.52±0.04	80.5±16.3
40124-01-35-00-c	1999-10-31, 08:22	09:11	SIMS	0.34±0.03	262.5±41.7
40124-01-36-00-a	1999-11-01, 03:26	04:23	SIMS	0.33±0.03	273.8±50.8
40124-01-36-00-b	1999-11-01, 05:02	05:59	SIMS	0.25±0.03	105.3±24.6
40124-01-37-01	1999-11-02, 01:50	02:25	SIMS	0.36±0.04	241.4±80.7
40124-01-37-02-a	1999-11-02, 06:37	07:32	SIMS	0.23±0.02	327.4±54.6
40124-01-38-00-b	1999-11-02, 21:26	21:51	SIMS	0.34±0.04	23.9±20.4
40124-01-41-00	1999-11-05, 00:13	01:20	SIMS	0.60±0.02	30.7±21.0
40124-01-44-00-a	1999-11-08, 11:24	12:05	SIMS	0.31±0.03	157.8±36.7
40124-01-48-01	1999-11-13, 14:25	15:01	SIMS	0.19±0.02	67.2±40.9
40124-01-50-00	1999-11-16, 07:42	08:19	SIMS	0.37±0.03	105.5±20.5
40124-01-53-01	1999-11-27, 07:12	07:53	soft state ⁽²⁾	0.30±0.03	165.4±33.0
40124-01-60-01	1999-12-28, 18:44	19:39	SIMS	0.27±0.03	61.4±34.3
40124-01-61-00	2000-01-03, 00:52	02:29	SIMS	0.15±0.02	402.8±62.0
Soft lags					
40124-01-13-00	1999-10-16, 23:04	23:34	SIMS	0.46±0.05	-83.6±29.1
40122-01-01-01	1999-10-18, 05:25	06:22	SIMS	0.31±0.04	-235.7±41.7
40124-01-16-00	1999-10-18, 11:50	12:40	SIMS	0.56±0.04	-27.4±21.6
40124-01-23-01	1999-10-22, 21:22	21:40	SIMS	0.50±0.08	-31.9±17.4
40124-01-26-00-a	1999-10-24, 03:42	04:40	SIMS	0.26±0.02	-361.6±40.5
40124-01-26-00-b	1999-10-24, 05:17	06:17	SIMS	0.36±0.04	-17.3±14.4
40124-01-28-00	1999-10-25, 10:17	11:04	SIMS	0.63±0.09	-19.4±6.9
40124-01-28-01	1999-10-25, 12:01	12:23	SIMS	0.36±0.05	-82.8±50.9
40124-01-29-00	1999-10-26, 03:38	04:49	SIMS	0.41±0.03	-217.8±31.6
40124-01-34-00-b	1999-10-30, 01:54	02:52	SIMS	0.53±0.04	-56.8±27.5
40124-01-34-01	1999-10-30, 08:26	09:06	SIMS	0.20±0.04	-60.7±26.9
40124-01-35-00-b	1999-10-31, 06:41	07:36	SIMS	0.39±0.03	-235.8±38.6
40124-01-38-00-c	1999-11-02, 22:31	23:29	SIMS	0.52±0.04	-60.4±22.6
40124-01-38-01	1999-11-03, 01:48	02:35	SIMS	0.84±0.02	-12.6±3.7
40124-01-39-00-c	1999-11-03, 22:30	23:29	SIMS	0.50±0.03	-133.9±32.7
40124-01-40-00	1999-11-04, 19:51	20:16	SIMS	0.31±0.09	-67.9±24.3
40124-01-45-00	1999-11-09, 09:43	10:30	SIMS	0.40±0.04	-168.5±34.9
40124-01-51-02-a	1999-11-21, 04:17	05:13	SIMS	0.16±0.02	-204.8±57.1
40124-01-55-00	1999-12-03, 05:20	05:59	SIMS	0.32±0.04	-34.7±26.9
40124-01-63-00	2000-01-17, 03:23	04:56	SIMS	0.21±0.02	-160.6±42.7
Without time lags					
40122-01-02-00-b	1999-10-27, 21:00	21:22	SIMS	0.27±0.06	-13.6±29.7
40122-01-02-00-c	1999-10-27, 22:37	23:03	SIMS	0.26±0.04	-9.8±31.9
40124-01-36-01	1999-10-31, 22:42	23:06	SIMS	0.38±0.03	12.6±13.6

Notes. The date, state of the detected positive correlations on the HID, cross-correlation coefficient and time lag of each observation are listed. The segments (> 1000 s) of an observation are labeled by ‘a’, ‘b’, and so on.

⁽¹⁾The total rms of the PDS ranges from 24% to 30%, the QPO frequency ranges from 0.46 Hz to 1.19 Hz, the photon index ranges from 1.6 to 2.1, the disk temperature ranges from 0.83 keV to 1.01 keV, and the fold energy ranges from 53 keV to 114 keV (Radhika & Nandi 2014).

⁽²⁾The total rms of the PDS ranges from 1% to 2%, the photon index remains ~ 2.2 , the disk temperature ranges from 0.7 keV to 0.9 keV (Radhika & Nandi 2014).

Table 3 Percentages of anti-correlations and positive correlations for each spectral state and the whole outburst.

Correlation/Lag	Hard state	HIMS	SIMS	Soft state	Whole outburst
Positive (%)	16.7	10.0	37.6	14.3	33.6
Anti (%)	0	20.0	6.0	0	6.4
Ambiguous (%)	83.3	70.0	56.4	85.7	60.0

in Fig. 7. The time lags in anti-correlation observations are longer than that in positive correlation observations, as shown in Fig. 8. To clearly present the evolution of the cross-correlations and time lags along with the spectral states, we show the segment percentage for CCCs and time lags of all the segments for each state in the top panel in Figs. 9 and 10, respectively. The numbers of segments with positive correlations, anti-correlations and ambiguous correlations are shown in the bottom panel of Fig. 9. The numbers of segments with anti-correlated time lag and positive correlated time lag are shown in the bottom panel of Fig. 10.

To study the change of the spectral parameters during the observations with hard lags, we take two segments (40124-01-34-00-a, 40124-01-35-00-a) showing anti-correlated hard lag or positive correlated hard lag to perform the spectra analysis, and we follow Sriram et al. (2007) by extracting the spectrum of two different time intervals (initial and final 300 s) of the observation. For the PCA spectral fitting, 0.5% systematic errors are added to the spectra, the hydrogen column density N_H is fixed at $0.6 \times 10^{22} \text{ cm}^{-2}$, the model that consists of a multi-color disk component, a power-law component and a Gaussian component is used, i.e., `wabs(diskbb+powerlaw+gauss)` (Sriram, Rao, & Choi 2013), and the centroid energy of Gaussian component is fixed at 6.4 keV. For the segment with anti-correlation, the unabsorbed disk flux has an opposite change with the unabsorbed power-law flux. The ObsID 40124-01-34-00-a shows anti-correlated hard X-ray lag, in which the disk flux increases while the power-law flux decreases, and the spectral analysis in 4U 1630-47 (Sriram et al. 2007) shows the same result. While the segment with positive correlation does not show this phenomenon (see Table 5). From Table 5, we can note that the inner disk radius ($\propto N_{bb}^{1/2}$) has change. Fig. 11 shows the unfolded spectra of part A (initial part) and part B (final part) of the two selected segments for spectral analyses.

4 DISCUSSION

Positive correlations are common in XRBs and easily understood. Hard X-ray emission comes from the inverse Compton scattering (ICS) of soft seed photons, so

the hard X-ray flux changes along with the increase or decrease of soft X-ray flux in general. Therefore, the following discussion will concentrate on anti-correlations.

4.1 Comparison with other XRBs

For XTE J1859+226, anti-correlations are detected in the IMS, viz., HIMS and SIMS, and the most are in the SIMS. Anti-correlations are also detected in the IMS of other five BHXBs which are GRS 1915+105, XTE J1550-564, 4U 1630-47, H1743-322 and GX 339-4. However, for BHXB Cyg X-3, anti-correlations are only detected in the hard state. In a word, anti-correlations are not found in the soft state of BHXBs.

However, anti-correlations are detected in every branch or state of NS LMXBs. Z-sources show Z-shaped tracks in CCDs along three branches, which are called horizontal branch (HB), normal branch (NB), and flaring branch (FB), respectively. The atoll sources show island state (IS) and banana state (BS) in CCDs, and BS can be subdivided into three states, viz., lower left banana (LLB), lower banana (LB), and upper banana (UB) states. Anti-correlations are found in HB, NB and FB of three Z-sources, viz., Cyg X-2 (Lei et al. 2008), GX 5-1 (Sriram, Choi, & Rao 2012) and XTE J1701-462 (Wang et al. 2014). For the atoll source, the anti-correlated observations are detected in the LB and UB of 4U 1735-44 (Lei et al. 2013), and in the IS, LLB and UB of 4U 1608-52 (Lei et al. 2014). In summary, anti-correlations are not detected in the soft state of BHXBs, but in every branch or state of NS LMXBs. This may be due to the spectra being dominated by the soft component in the soft state of BHXBs, while the soft seed photons in BHXBs only originate from the accretion disk but from both the accretion disk and the surface of the NS for NS LMXBs.

For the observations with anti-correlations in BHXBs, hard lags are generally found. For XTE J1859+226, the anti-correlated hard lags are detected in the SIMS, and that lags range from ~ 204 to ~ 953 seconds. For Cyg X-3, the anti-correlated hard lags are detected in the hard state, which range from ~ 620 to ~ 950 seconds (Choudhury & Rao 2004). The anti-correlated hard lags are detected in the IMS of GRS 1915+105 (Choudhury et al.

2005), XTE 1550-564 (Sriram et al. 2007) and H1743-322 (Sriram, Agrawal, & Raghurama Rao 2009), which range from ~ 128 to ~ 1600 seconds, ~ 132 to ~ 376 seconds and ~ 442 to ~ 1591 seconds, respectively. From the above results, it is easy to note that the ranges of anti-correlated hard lags detected in different BHXBs are similar.

Anti-correlated soft lags are first found in the IMS of GX 339-4 which range from ~ 95 to ~ 1068 seconds (Sriram, Rao, & Choi 2010). XTE J1859+226 is the second BHXB that shows anti-correlated soft lags that range from ~ 120 to ~ 718 seconds. The ranges of anti-correlated soft lags detected in these two BHXBs do not differ significantly. Table 4 shows all the ranges for time lags detected in BHXBs.

We notice that the time lags in anti-correlation observations of XTE J1859+226 are longer than that in positive correlation observations (see Fig. 8). This phenomenon is also detected in atoll source 4U 1608-52 (Lei et al. 2014) and Z-source GX 349+2 (Ding et al. 2016). However, for atoll source 4U 1735-44 (Lei et al. 2013) and Z-source XTE J1701-462 (Wang et al. 2014), the length of time lags in positive correlation observations does not show obvious difference from that in anti-correlation observations.

It is interesting to note that the proportion of anti-correlated soft lags and anti-correlated hard lags does not show obvious relation with the category of source. Of the observations of XTE J1859+226 that show anti-correlations, the percentage of observations with soft lags (78%) is more than that with hard lags (22%), as shown in the bottom panel of Fig. 10. GX 349+2 (Z-source) shows the same phenomenon (Ding et al. 2016), while the opposite is detected in Z-source Cyg X-2 (Lei et al. 2008), Z-source GX 5-1 (Sriram, Choi, & Rao 2012), Z-source XTE J1701-462 (Wang et al. 2014), atoll source 4U 1735-44 (Lei et al. 2013) and atoll source 4U 1608-52 (Lei et al. 2014).

4.2 Explanation of the Results in XTE J1859+226

Model-independent spectral pivoting is detected in the anti-correlated observations of BHXB XTE J1859+226, this spectral pivoting is the strongest evidence for the anti-correlation (Choudhury et al. 2003; Choudhury & Rao 2004), and this kind of spectral pivoting has been detected in the anti-correlated observations of six BHXBs (Cyg X-3 (Choudhury & Rao 2004), GRS 1915+105 (Choudhury et al. 2005), XTE J1550-564 and 4U 1630-47 (Sriram et al. 2007), H1743-322 (Sriram, Agrawal, & Raghurama Rao 2009) and GX 339-4 (Sriram, Rao, & Choi 2010)) and five NS LMXBs (Cyg X-2 (Lei et al. 2008), GX 5-1

(Sriram, Choi, & Rao 2012), 4U 1735-44 (Lei et al. 2013), 4U 1608-52 (Lei et al. 2014) and XTE J1701-462 (Wang et al. 2014)). However, spectral pivoting is not detected in the positively correlated observations of XTE J1859+226, and the same result is found in the above five NS LMXBs. This kind of model-independent spectral pivoting behavior might imply that the radiation mechanism and spectral properties are different in the anti-correlated observations and positively correlated observations.

For XTE J1859+226, both anti-correlations and positive correlations are found in the first 100 days (out of 166 days) when the luminosity is high. The number of observations with anti-correlations or positive correlations begins to decrease from the 40th day of the whole outburst (see Fig. 6). These results imply that the distribution of cross-correlations may be related to the high luminosity of the BHXB. Positive correlations do not show clear evolution with hardness ratio in the HID, whereas anti-correlations are detected in the observations with moderate hardness ratio, as illustrated by the Fig. 7. Therefore, anti-correlations may be related to the moderate hardness ratio in BHXB.

Anti-correlated lags detected in XTE J1859+226, which range from ~ 120 to ~ 953 seconds, are long time-scale lags (longer than 1 second). The short time-scale X-ray lags, of less than 1 second, observed in XRBs can be explained by Comptonization model (Lee, Misra, & Taam 2001) and shot model (van der Klis et al. 1987; Miyamoto & Kitamoto 1989; Nowak, Wilms, & Dove 1999). However, these models can not explain the long-term time lags detected in BHXB, which range from hundreds to thousands of seconds. The truncated accretion disk model is invoked to interpret the anti-correlated long time-scale hard X-ray lags detected in the hard state of BHXB Cyg X-3 (Choudhury & Rao 2004). In this model, the accretion disk is truncated far away from the compact object. The high-temperature Comptonizing cloud is constrained to the area between the truncated disk and the compact object. The accretion disk front moves inward (outward), leading to a decrease (increase) of the Comptonizing cloud. Any changes in the accretion disk will result in opposite changes in the Comptonizing cloud resulting in anti-correlated hard X-ray lags corresponding to the viscous timescale of the readjustment of the accretion disk.

The truncated accretion disk model is widely used to explain similar hard X-ray lags in BHXBs (GRS 1915+105 (Choudhury et al. 2005), XTE J1550-564 and 4U 1630-47 (Sriram et al. 2007), H1743-322 (Sriram, Agrawal, & Raghurama Rao 2009)) and NS LMXBs (Cyg X-2 (Z-source) (Lei et al. 2008), GX

Table 4 XTE J1859+226 and other twelve XRBs in which long time-scale lags are detected and their ranges of time lags.

Object	Range of AS Lag (s)	Range of AH Lag (s)	Range of PS Lag (s)	Range of PH Lag (s)
Z-source				
Cyg X-2 (1)	$-35 \pm 25 \sim -184 \pm 29$	$46 \pm 14 \sim 376 \pm 25$
GX 5-1 (2)	$-160 \pm 70 \sim -920 \pm 102$	$31 \pm 12 \sim 748 \pm 62$
XTE J1701-462 (3)	$-29 \pm 15 \sim -1278 \pm 30$	$54 \pm 14 \sim 1138 \pm 26$	$-9 \pm 6 \sim -1334 \pm 15$	$17 \pm 10 \sim 1300 \pm 23$
GX 349+2 (4)	$-66 \pm 10 \sim -6107 \pm 46$	$85 \pm 6 \sim 1177 \pm 57$	$-3.9 \pm 3.2 \sim -286 \pm 40$	$2.8 \pm 1.8 \sim 136 \pm 27$
atoll source				
4U 1735-44 (5)	$-26 \pm 25 \sim -350 \pm 10$	$63 \pm 33 \sim 152 \pm 28$	$-14 \pm 5 \sim -337 \pm 19$	$25 \pm 15 \sim 368 \pm 24$
4U 1608-52 (6)	-100 ± 102	$168 \pm 32 \sim 628 \pm 43$	$-13 \pm 10 \sim -50 \pm 44$	$19 \pm 19 \sim 248 \pm 77$
BHXB				
Cyg X-3 (7)	...	$620 \pm 70 \sim 950 \pm 60$
GRS 1915+105 (8)	...	$128 \pm 30 \sim 1600 \pm 200$
XTE 1550-564 (9)	...	$132 \pm 9 \sim 376 \pm 14$
4U 1630-47 (9)	...	363 ± 48
H1743-322 (10)	...	$442 \pm 38 \sim 1591 \pm 58$
GX 339-4 (11)	$-95 \pm 40 \sim -1068 \pm 62$
XTE J1859+226	$-120 \pm 16 \sim -718 \pm 75$	$204 \pm 87 \sim 953 \pm 65$	$-12.6 \pm 3.7 \sim -362 \pm 41$	$12.1 \pm 3.7 \sim 403 \pm 62$

Notes. AS Lag: anti-correlated soft lag

AH Lag: anti-correlated hard lag

PS Lag: positive correlated soft lag

PH Lag: positive correlated hard lag

References: (1) Lei et al. (2008), (2) Sriram, Choi, & Rao (2012), (3) Wang et al. (2014), (4) Ding et al. (2016), (5) Lei et al. (2013), (6) Lei et al. (2014), (7) Choudhury & Rao (2004), (8) Choudhury et al. (2005), (9) Sriram et al. (2007), (10) Sriram, Agrawal, & Raghurama Rao (2009) and (11) Sriram, Rao, & Choi (2010).

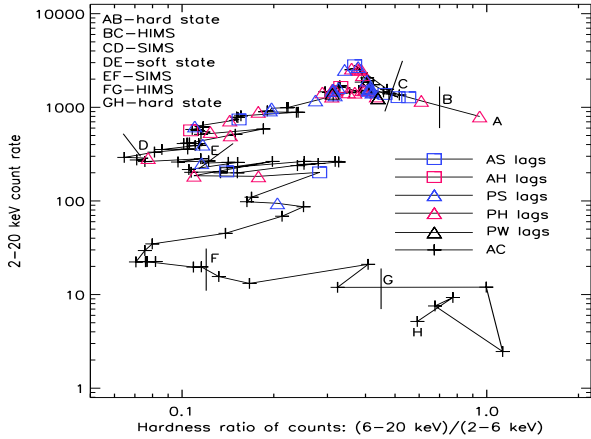


Fig. 7 The results of cross-correlation and time lag from the PCA observation, and the anti-correlated soft (AS) lag, anti-correlated hard (AH) lag, positive correlated soft (PS) lag, positive correlated hard (PH) lag, positive correlation without (PW) time lag and ambiguous correlation (AC) segments, as shown in the legend.

5-1 (Z-source) (Sriram, Choi, & Rao 2012), 4U 1735-44 (atoll source) (Lei et al. 2013), 4U 1608-52 (atoll source) (Lei et al. 2014), XTE J1701-462 (Z-source) (Wang et al. 2014)). Spectral analysis shows that the inner disk radius ($\propto N_{bb}^{1/2}$) is changing, and this could be the evidence of the movement of accretion disk front (see Table 5). Therefore, we suggest that the anti-correlated hard X-ray lags detected in XTE J1859+226 are also produced by that mechanism.

Anti-correlated soft X-ray lags can also be interpreted in the framework of the truncated accretion disk model. Li, Xue, & Lu (2007) suggested that the fluctuation produced in the innermost region of the BH accretion disk expands and propagates to the outer region of accretion disk, that fluctuation heats up the inner material and disturbs the outer material, and that fluctuation lasts within thousands of seconds for the accretion disk with Stellar-Mass Black Hole. Lei et al. (2008) invoked that fluctuation to explain the anti-correlated soft lags detected in Cyg X-2 (Z-source), and that fluctuation mechanism was also adopted to interpret similar soft lags detected in Z-source GX 5-1 (Sriram, Choi, & Rao 2012), atoll source 4U 1735-44 (Lei et al. 2013) and Z-source XTE J1701-462 (Wang et al. 2014). Sriram, Rao, & Choi (2010) detected anti-correlated long time-scale soft X-ray lags in the IMS of BHXB GX 339-4 and they suggested that the temporal and spectral variations during the soft lag timescale could be explained with the framework of the truncated accretion disk model. XTE

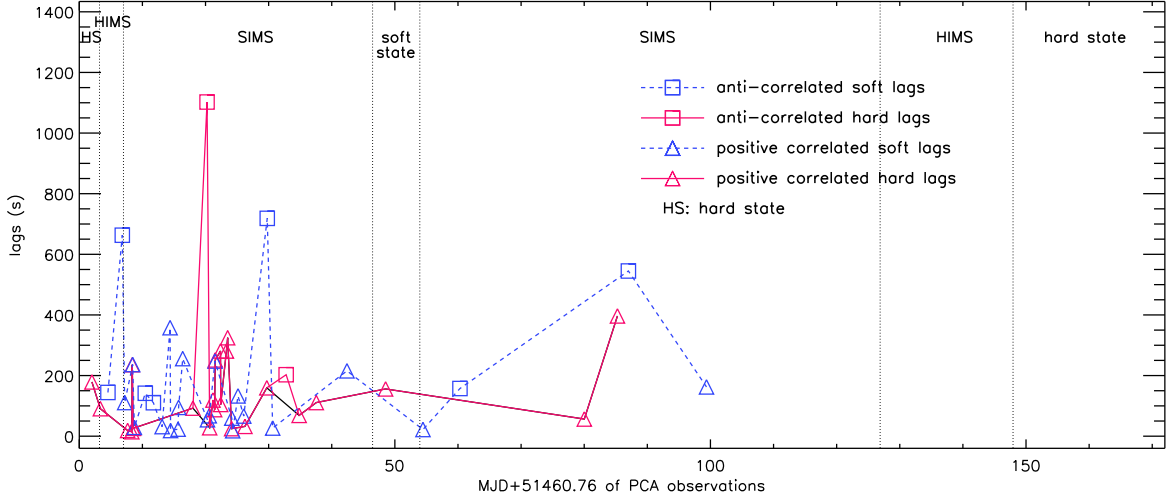


Fig. 8 Soft lags and hard lags vs. MJD for the anti-correlated soft lag, anti-correlated hard lag, positive correlated soft lag and positive correlated hard lag, as shown in the legend.

Table 5 Best-fitting parameters for part A (initial part) and part B (final part) spectral of the two selected segments for spectral analyses.

Parameters	40124-01-34-00-a		40124-01-35-00-a	
	A	B	A	B
kT_{in}^a	$0.84^{+0.01}_{-0.01}$	$0.85^{+0.01}_{-0.01}$	$0.83^{+0.01}_{-0.01}$	$0.85^{+0.01}_{-0.01}$
N_{bb}^b	752^{+39}_{-38}	840^{+45}_{-42}	802^{+43}_{-40}	896^{+46}_{-44}
Γ_{Pl}^c	$2.52^{+0.03}_{-0.02}$	$2.48^{+0.01}_{-0.01}$	$2.56^{+0.02}_{-0.02}$	$2.47^{+0.02}_{-0.02}$
Disk flux ^d	$1.88^{+0.05}_{-0.05}$	$2.14^{+0.08}_{-0.07}$	$2.12^{+0.04}_{-0.03}$	$2.18^{+0.04}_{-0.05}$
Power-law flux	$4.28^{+0.06}_{-0.06}$	$3.85^{+0.08}_{-0.08}$	$3.11^{+0.06}_{-0.05}$	$3.11^{+0.06}_{-0.06}$
$Flux_{total}$	6.25	6.09	5.33	5.39
Disk flux/ $Flux_{total}^e$	30.08%	35.14%	39.77%	40.45%
χ^2/dof	42/51	52/51	53/51	52/51

Notes. The model $wabs(\text{diskbb}+\text{powerlaw}+\text{gauss})$ is used, and all the quoted errors are at a 90 percent confidence level.

^aInner disk temperature of diskbb model.

^bNormalization of discbb model.

^cPower-law index.

^dFor all the models, the flux unit is $10^{-9}\text{ergs cm}^{-2}\text{s}^{-1}$, and fluxes are unabsorbed in 2.8–30 keV energy band.

^eThe ratio of the disk flux to the total flux.

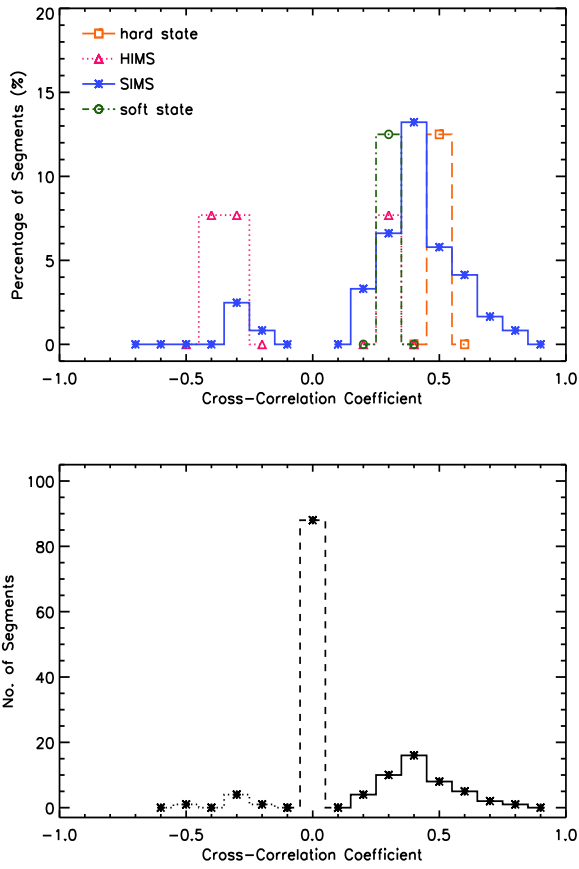


Fig. 9 Top panel: the percentage of segments with CCCs. Bottom panel: the CCCs of the anti-correlations (dotted line), positive correlations (solid line) and ambiguous correlations (dashed line) vs. the number of segments.

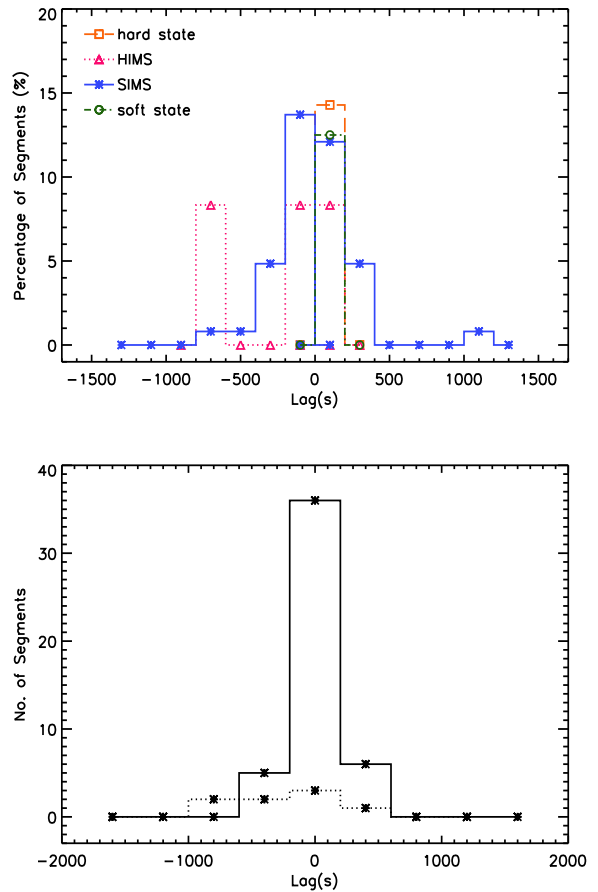


Fig. 10 Top panel: percentage of segments vs. time lags. Bottom panel: the time lags of the anti-correlations (dotted line), positive correlations (solid line) vs. the number of segments.

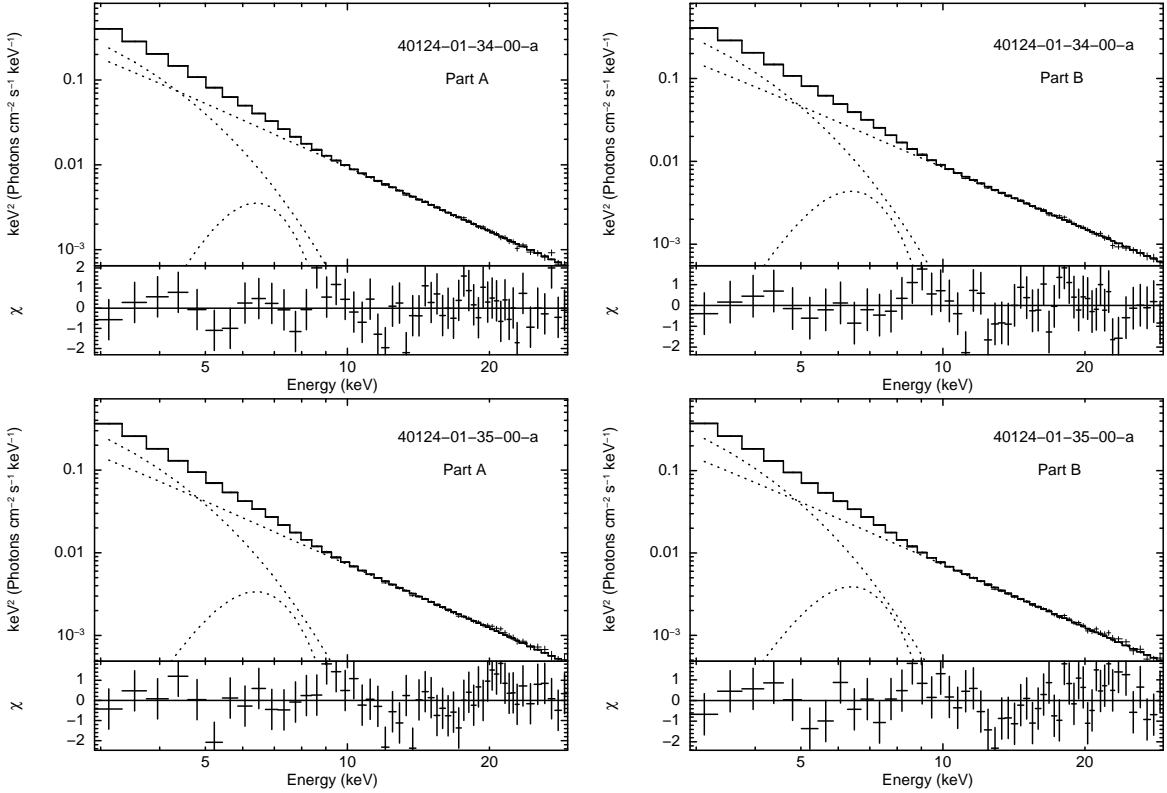


Fig. 11 Unfolded spectra and the corresponding $\Delta\chi$ of the two selected segments for spectral analyses, using the model of wabs(diskbb+powerlaw+gauss). A and B correspond to the initial and final parts of the segments.

J1859+226 is the second BHXB in which the anti-correlated long time-scale soft X-ray lags are detected. We suggest that, in the framework of the truncated accretion disk model, this fluctuation mechanism can explain the anti-correlated long time-scale soft X-ray lags detected in BHXB as well. Considering the anti-correlated long time-scale X-ray lags are detected in IMS of XTE J1859+226 but never in the soft state of BHXB, we suggest that the accretion disk is truncated at the IMS of BHXB but may be not truncated at soft state.

The proportion of multi-color disk component in the segment with positive correlation is higher than that in the segment with anti-correlation (see Table 5). Therefore, soft seed thermal photons emitted in the accretion disk dominate the cross-correlations between the soft and hard X-rays during the observations with positive correlation, i.e., the decrease or increase of soft seed thermal photons will lead to a same change in the hard X-ray emission. The relative changes in inner disk radius observed from the spectral fits are just close to 90% confidence level (Table 5) and resolved spectral observations are required in order to constrain the changes during the anti-correlated observations. In addition, the change of inner disk radius ($\propto N_{bb}^{1/2}$) has the similar amplitude during the segments with posi-

tive correlation and anti-correlation (see Table 5). We suggest that the positive correlated hard lags may correspond to the viscous timescale of the readjustment of the accretion disk as anti-correlated hard lags, and the positive correlated soft lags may result from the fluctuation as anti-correlated soft lags for BHXBs.

5 CONCLUSION

Using the data from RXTE for the BHXB XTE J1859+226 during its entire 1999–2000 outburst, we perform a systematic study of the CCF and time lag between the soft and hard X-rays. For the first time, positive correlated soft lags and hard lags detected in BHXB are reported. Anti-correlated soft lags are second observed in BHXB, and anti-correlated hard lags are also observed in BHXB XTE J1859+226. Anti-correlations are detected in every branch or state of NS LMXBs, but never detected in the soft state of BHXBs. This may be due to the soft seed photons in NS LMXBs and BHXBs being emitted from different regions. The timescales of anti-correlated hard lags detected in different BHXBs do not show obvious difference, where the timescales range from several hundreds to more than one thousand seconds. The ranges

of anti-correlated soft lags detected in XTE J1859+226 and BHXB GX 339-4 do not have obvious difference. In XTE J1859+226, the time lags detected in anti-correlation observations are longer than that in positive correlation observations. In the observations with anti-correlations, most of the lags are soft lags. The proportion of the observations with anti-correlated soft lags and hard lags does not display obvious relation with the source type. Anti-correlations and positive correlations and their respective soft and hard X-ray lags are only detected in the first 100 days of the outburst when the luminosity or the accretion rate are high implying that the cross-correlations between the soft and hard X-rays may be related to the high luminosity. We suggest that anti-correlated long time-scale X-ray hard lag and soft lag can be explained by combination of the truncated accretion disk model and a fluctuation that propagates from the inner disk to the outer disk. The anti-correlated long time-scale X-ray lags are never found in the soft state of BHXBs probably because the accretion disk is not truncated at soft state.

Acknowledgements

We thank the anonymous referee for her or his constructive comments and suggestions, which helped us to carry out this research deeply and improve the presentation of this paper. This research has made use of the data obtained through the High Energy Astrophysics Science Archive Research Center (HEASARC) On-line Service, provided by NASA/Goddard Space Flight Center (GSFC). This work is partially supported by the National Program on Key Research and Development Project (Grant Nos. 2016YFA0400804 and 2016YFA0400803) and the National Key Basic Research Program of China (973 Program 2015CB857100). This work is also partially supported by the Natural Science Foundation of China (Grant Nos. 11303047, 11573059 and 11673023) and the 2014 Project of Xinjiang Uygur Autonomous Region of China for Flexibly Fetching in Upscale Talents.

References

- Belloni T. M., 2010, LNP, 794, 53
 Choudhury M., Rao A. R., 2004, ApJ, 616, L143
 Choudhury M., Rao A. R., Dasgupta S., Pendharkar J., Sriram K., Agrawal V. K., 2005, ApJ, 631, 1072
 Choudhury M., Rao A. R., Vadawale S. V., Jain A. K., 2003, ApJ, 593, 452
 Colpi M., Casella P., Gorini V., Moschella U., Possenti A., 2009, ASSL, 359,
 Corral-Santana J. M., Casares J., Shahbaz T., Zurita C., Martínez-Pais I. G., Rodríguez-Gil P., 2011, MNRAS, 413, L15
 Cui W., Shrader C. R., Haswell C. A., Hynes R. I., 2000, ApJ, 535, L123
 Debnath D., Chakrabarti S. K., Nandi A., Mandal S., 2008, BASI, 36, 151
 Ding G. Q., Zhang W. Y., Wang Y. N., Li Z. B., Qu J. L., Huang C. P., 2016, MNRAS, 455, 2959
 Done C., Gierliński M., Kubota A., 2007, A&ARv, 15, 1
 Dunn R. J. H., Fender R. P., Körding E. G., Belloni T., Cabanac C., 2010, MNRAS, 403, 61
 Farinelli R., et al., 2013, MNRAS, 428, 3295
 Hasinger G., van der Klis M., 1989, A&A, 225, 79
 Homan J., Belloni T., 2005, Ap&SS, 300, 107
 Hynes R. I., Haswell C. A., Chaty S., Shrader C. R., Cui W., 2002, MNRAS, 331, 169
 Lee H. C., Misra R., Taam R. E., 2001, ApJ, 549, L229
 Lei Y. J., et al., 2008, ApJ, 677, 461-472
 Lei Y.-J., et al., 2013, AJ, 146, 60
 Lei Y.-J., et al., 2014, AJ, 147, 67
 Lewin W. H. G., van der Klis M., 2006, csxs.book, 39,
 Li S.-L., Xue L., Lu J.-F., 2007, ApJ, 666, 368
 Markoff S., Nowak M. A., 2004, ApJ, 609, 972
 Markoff S., Nowak M. A., Wilms J., 2005, ApJ, 635, 1203
 Markwardt C. B., Marshall F. E., Swank J. H., 1999, IAUC, 7274, 2
 McClintock J. E., Remillard R. A., 2006, csxs.book, 39, 157
 Miyamoto S., Kitamoto S., 1989, Natur, 342, 773
 Motta S., Belloni T., Homan J., 2009, MNRAS, 400, 1603
 Nandi A., Debnath D., Mandal S., Chakrabarti S. K., 2012, A&A, 542, A56
 Nowak M. A., Wilms J., Dove J. B., 1999, ApJ, 517, 355
 Radhika D., Nandi A., 2014, AdSpR, 54, 1678
 Rau A., Greiner J., 2003, A&A, 397, 711
 Remillard R. A., 2005, AIPC, 797, 231
 Remillard R. A., McClintock J. E., 2006, ARA&A, 44, 49
 Shaposhnikov N., Titarchuk L., 2009, ApJ, 699, 453
 Sriram K., Agrawal V. K., Pendharkar J. K., Rao A. R., 2007, ApJ, 661, 1055
 Sriram K., Agrawal V. K., Raghurama Rao A., 2009, RAA, 9, 901
 Sriram K., Choi C. S., Rao A. R., 2012, ApJS, 200, 16
 Sriram K., Rao A. R., Choi C. S., 2010, ApJ, 725, 1317
 Sriram K., Rao A. R., Choi C. S., 2013, ApJ, 775, 28
 Timmer J., Koenig M., 1995, A&A, 300, 707
 van der Klis M., Hasinger G., Stella L., Langmeier A., van Paradijs J., Lewin W. H. G., 1987, ApJ, 319, L13
 Wang Y. N., Lei Y. J., Ding G. Q., Qu J. L., Ge M. Y., Zhang C. M., Chen L., Ma X., 2014, MNRAS, 440, 3726
 Wood A., Smith D. A., Marshall F. E., Swank J., 1999, IAUC, 7274, 1
 Zurita C., et al., 2002, MNRAS, 334, 999